

# Universal Approach to Direct Spatiotemporal Dynamic *in-situ* Optical Visualization of On-Catalyst Water Splitting Electrochemical Processes

Gaurav Bahuguna<sup>1\*</sup>, Fernando Patolsky<sup>1,2\*</sup>

<sup>1</sup>*School of Chemistry, Faculty of Exact Sciences, Tel Aviv University, Tel Aviv, 69978, Israel.*

<sup>2</sup>*Department of Materials Science and Engineering, the Iby and Aladar Fleischman Faculty of Engineering, Tel Aviv University, Tel Aviv 69978, Israel.*

\**Corresponding Authors:*

Prof. Fernando Patolsky ([fernando@post.tau.ac.il](mailto:fernando@post.tau.ac.il))

Dr. Gaurav Bahuguna ([gauravb@tauex.tau.ac.il](mailto:gauravb@tauex.tau.ac.il), [bahuguna.1@itj.ac.in](mailto:bahuguna.1@itj.ac.in))

## Abstract

Electrochemical reactions are the unrivaled backbone of next generation energy storage, energy conversion and healthcare devices. However, the *in-situ* real-time visualization of electrochemical reactions, which can shed light on various critical unknown insights on the electrochemical processes, still remains the bottleneck for fully exploiting their intrinsic potential. In this work, for the first time, a universal approach to the direct spatiotemporal-dynamic *in-situ* optical visualization of pH based as well as specific byproduct based electrochemical reactions is performed. As a highly relevant and impactful example, the *in-operando* optical visualization of on-catalyst water splitting processes is performed under neutral water/seawater conditions. pH based visualization are performed using a water-soluble fluorescent pH probe HPTS (8-hydroxypyrene-1,3,6-trisulfonic acid), known for its exceptional optical capability of detecting even the tiniest environment pH changes, thus allowing the unprecedented “spatiotemporal” real-time visualization at the cathode and anode. The successful experimental investigations embarked here, allowed us to reach several yet unveiled deeper insights into the spatiotemporal water splitting processes and their practical modulation for potentially improving the applicability and efficiency of water splitting devices. As a result, we were able to unprecedentedly reveal that at a critical cathode-to-anode distance, a continuous bulk-electrolyte “self-neutralization” phenomenon can be achieved during the water splitting process, leading to the practical realization of enhanced additive-free neutral water splitting. Furthermore, we experimentally unveiled that at increasing electrolyte flow rates, a swift and severe inhibition of the concomitantly forming acidic and basic ‘fronts’, developed at anode and cathode compartments is observed, thus acting as a continuous on-catalysts “buffering” mechanism that allows for a remarkably enhanced water splitting process.

Furthermore, to demonstrate the universal applicability of this elegant strategy which is not limited to pH changes, the technique was extended to visualization of specific electrochemical process by the use of reaction product-specific fluorophore. For the purpose, N-(4-butanoic acid) dansylsulfonamide (BADs) fluorophore was successfully explored to in-situ visualize the formation of hypochlorite/ chlorine at the anode during electrolysis of sea water. Thus, a unique experimental tool that allow real-time spatiotemporal visualization and simultaneous mechanistic investigation of complex electrochemical processes in developed that can be universally extended to various fields of research.

**Keywords:** *visualizing water splitting, in operando analysis, HPTS, confocal microscopy, spatiotemporal dynamic analysis.*

## Introduction

Electrochemistry is one of the most important domains of science and is known since decades for its immense applicability in various field of interest. It has a widespread application in the present day most important areas of energy<sup>1-5</sup> and healthcare<sup>6-11</sup>. As a result, this high impact research field has since its discovery received enormous research attention and efforts, with continuous accomplishment of fundamental and technological developments<sup>12-14</sup>. In spite of these significant research achievements, the field of electrochemistry is still far from fulfilling its intrinsic potential, with the scope of still accomplishing tremendous future developments. These developments can lead to the evolution of next-generation energy storage, energy conversion and healthcare devices for a sustainable and healthy development of mankind<sup>13-17</sup>. The comprehensive applicability of electrochemistry, and electrochemical reactions, is still restricted due to the current limited in-depth understanding, and lack of experimental tools for the in-depth characterization, of various electrochemical processes of interest. Thus, the discovery and development of novel and innovative scientific and technological avenues towards the understanding of complex electrochemical processes is highly desired and required<sup>18-20</sup>. Thus, the in-situ spatiotemporal “visualization” of electrochemical processes can represent a major breakthrough in this field of research, and may lead to unveiling yet unexposed fascinating insights in the field<sup>21</sup>. However, it is unfortunate that in-spite of major advancements in the development of optical microscopic techniques, the spatiotemporal dynamic ‘visualization’ of electrochemical reactions has not yet been demonstrated.

Fluorescence-based imaging techniques represent one of the central routes for achieving the goal of spatiotemporal visualization of electrochemical reactions<sup>22-27</sup>. Few reports are available

on the sensing of electrochemical reactions using a fluorophore that is responsive to any one of the reactions products<sup>28</sup>. This, however, requires the application of highly specific fluorophores for the specific product, and thus cannot be extended universally to different electrochemical processes<sup>28</sup>. Additionally, most of the works in literature report on the fluorescence sensing of the electrochemical products, rather than the in-situ imaging or visualization of any electrochemical reactions<sup>26,28</sup>. Furthermore, it is very important to provide the quantitative in-operando visualization of the electrochemical reactions, which is usually missing in existing literature investigations<sup>29</sup>. Acid/base (or pH) fluorescent probes can be one of the best candidates for visualization purposes, as most of the electrochemical reactions involve the oxidation or reduction of specific moieties which cause a concomitant decrease or increase in the environment pH, at one or both of the electrodes simultaneously<sup>30,31</sup>. These changes in pH can be monitored using an acid/base (pH)-sensitive fluorescent probe for monitoring the in-situ progress of any electrochemical reaction. The pH-based visualization of electrochemical reactions can be universally applied to various electrochemical processes, however, it presently suffers majorly due to limited range of suitable fluorescent probes displaying chemical and electrochemical stability in the voltage window of interest, the use of multiple fluorescent dyes for specific tasks and voltage range of interest, the lack of a suitable visualization approach, etc. which overall make the spatiotemporal visualization process very complex. Recently, Roberts et al.<sup>32</sup> used a combination of dyes to monitor an electrocoagulation process by observing the pH changes in the range of 1.5 to 8.5. To address these issues, we have explored HPTS (8-hydroxypyrene-1,3,6-trisulfonic acid) as a fluorescent probe, with a neutral pKa of 7.4 in the ground state. HPTS is a well-known photoacid molecular species, displaying a sharp transition from its pKa of 7.4 in the ground state, being a weak acid, to a pKa of ~0.5 in its photo-excited state, making it a strong acid upon excitation. The exceptional properties of the HPTS molecule allow it to monitor any minute changes from neutrality, to acidic or basic conditions, thus allowing the use of a single fluorescent probe. Furthermore, the optical fluorescence properties of the molecule allow the ratiometric sensing of the acid/basic transitions, and thus can be used for the reliable qualitative and quantitative analysis of any small changes in the environment.<sup>12,17,22–25,33,34</sup>

In the past few decades, electrocatalytic water splitting for hydrogen gas production was established as a basis for sustainable development, and has led to significant progress in terms of efficiency and achievable low overpotentials under alkaline/acidic conditions<sup>35–39</sup>. Corrosive environment, use of additives and expensive separators have very recently shifted the research

attention to the realization of neutral water splitting<sup>40-46</sup>. However, it is at an initial state and necessitates innovative characterization tools for better understanding of the electrocatalytic water splitting under unbuffered neutral conditions<sup>47</sup>. In this work, for the first time, direct spatiotemporal dynamic in-situ optical visualization of on-catalyst water splitting processes is performed under neutral condition by exploiting the exceptional fluorescent properties of the HPTS probe<sup>47</sup>. Under neutral conditions, the oxidation and reduction of water (for production of oxygen and hydrogen) at anode and cathode, respectively, leads to the formation of acidic and basic environments around the electrodes at neutral conditions<sup>48,49</sup>. This associated formation of acid and base ‘fronts’ leads to a decrease and increase in the pH, respectively, which can be optically visualized directly by the opto-electrochemical cell developed in this study<sup>50</sup>. Recently, Obata et al.<sup>50</sup> attempted bulk in-situ imaging of the water splitting process under neutral conditions, and successfully observed the concomitant formation of acid and base and its associated pH changes. However, the work involved the use of a fluorescent strip in between the two electrodes, which lead to limitations of minimum uncontrollable contact nature with the electrodes, resulting in contact aberrations, non-microscopic imaging capabilities with low-resolution and limited dimensional imaging, completely lacking 3D optical information of environmental chemical changes. Considering this broad research gap, the quest for a fluorescent probe is realized which can directly be added to the electrolyte medium for in-operando visualization of water splitting reactions. Thus, an opto-electrochemical cell, using HPTS as a fluorescent probe, was developed which demonstrates the following unprecedented advantages: (i) universal indicator for acid and base (pH) environment changes, (ii) direct homogeneous addition into the cell electrolyte, (iii) 3D spatial imaging capabilities, (iv) ratiometric fluorescence analysis and (v) easy qualitative and quantitative analysis in a single system. As a result, the opto-electrochemical cell developed in this work is successfully able to quantitatively visualize the spatiotemporal development of acidic and basic fronts at the anode and cathode surfaces during the water splitting process reactions. Furthermore, the ability of the opto-electrochemical cell to spatially visualize in-situ water splitting reactions was practically applied to unveil further key insights on the efficiency of unbuffered neutral water splitting. Specifically, the possibility of ‘self-neutralization’ via optimizing the distance gap between the electrodes, as well as the effect of applying different electrolyte “flow” conditions, at different flow rates, on the water splitting process were here investigated by in-situ opto-electrochemical imaging platform, under static and under-flow electrolyte conditions, leading to the experimental discovery of key new insights that allow further enhancing the water splitting process under neutral conditions. Additionally, this

approach was here universally applied for the spatiotemporal monitoring of chemical by-products other than pH changes, such as the formation of hypochlorite and chlorine species using a specific fluorophore, concomitantly produced during the sea water splitting process under neutral conditions. This shows the universal nature of our novel experimental paradigm that can be extended to any electrochemical reaction per se.

## Materials and Methods

To perform in-situ visualization of electrochemical measurements, the opto-electrochemical cell was fabricated with an optical glass window on its top face. Pre-cleaned nickel foil (99.99%) and platinum foil (99.99%) sheets were used as the electrode materials for the opto-electrochemical investigations. The distance between the optical glass window and electrodes surface is ~5mm, in order to cater the small working distance for the optical objectives used in this study, and allow changing the distance between the electrodes for different purposes. Furthermore, in order to perform electrolyte flow measurements, the cell is equipped with inlet and outlet ports connected to a syringe pump with adjustable flow rate. The electrolyte used in this work is 0.25 M Na<sub>2</sub>SO<sub>4</sub> with the co-addition of 10 μM HPTS (8-hydroxypyrene-1,3,6-trisulfonic acid) (Sigma, 6358-69-6). Dilute potassium hydroxide and dilute hydrochloric acid was used to make solutions with different pHs, using an Oakton pH analyser. As a control, 0.25 M phosphate buffer, with the co-addition of 10 μM HPTS, is also tested. Further, the opto-electrochemical detection of chloride oxidation was performed using 50 μM N-(4-butanoic acid) dansylsulfonamide (BADs) fluorophore by directly adding in the electrolyte (0.5 M NaCl in phosphate buffer). N-(4-butanoic acid) dansylsulfonamide 99%, CAS: 102783-77-7 was purchased Henan Bao Enluo Trading Co. Ltd, China. The operational opto-electrochemical imaging studies were performed using an inverted fluorescence Thunder microscope (LEICA MD4000M Fluorescence microscope with LEICA DFC450 camera), using the 395 nm and 440 nm as excitation wavelengths. The opto-electrochemical fluorescence images and movies were analysed using the Leica image analysis software (LAS X). The opto-electrochemical imaging was also performed at different electrode distances, and under varying electrolyte flow rates. The electrochemical measurements were performed in a two-electrode configuration, using a PalmSens electrochemical instrument.

## Results and Discussion

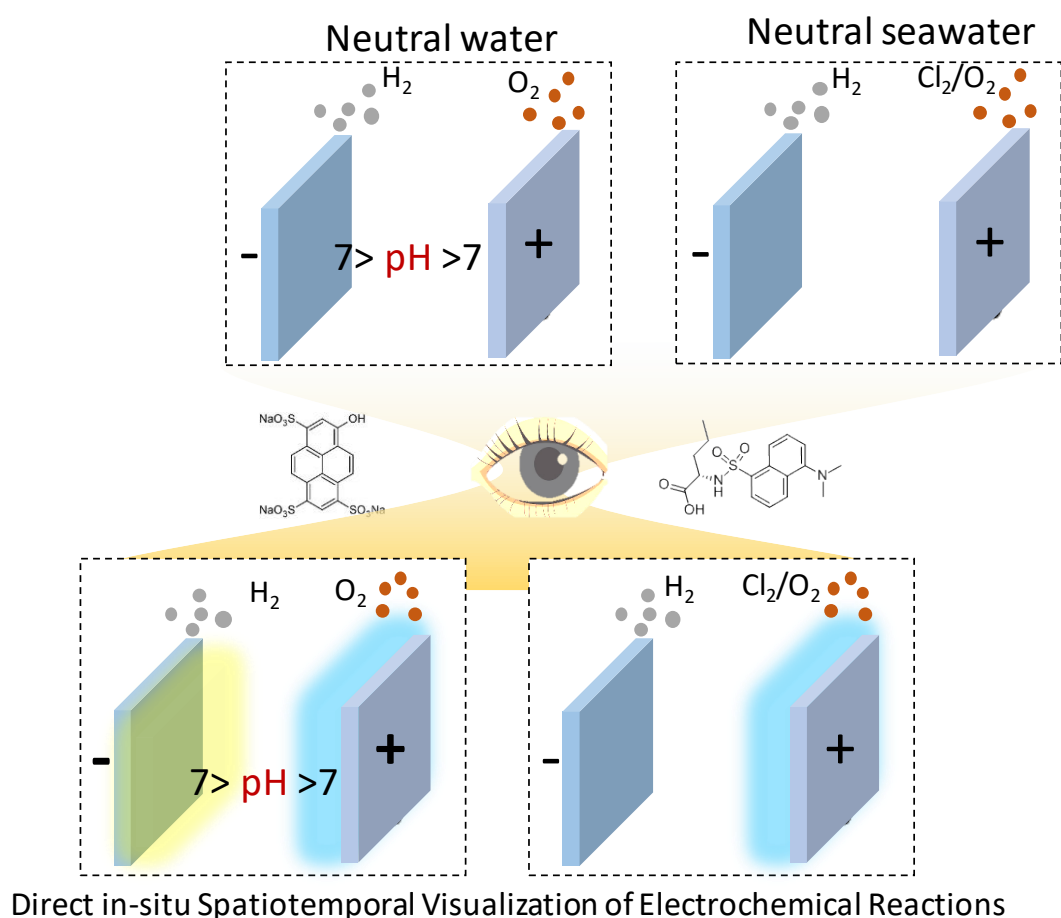


**Figure 1.** Schematic demonstration of the in-situ optical spatiotemporal visualization of electrochemical reactions, considering the cases of neutral water and neutral sea water splitting as an example.

It is now well known that the in-depth understanding of electrochemical processes is one of the most promising avenues for the achievement of major advancements in different emerging fields for future development. In conjunction, in this work, we have developed opto-electrochemical technique than can be explored universally for visualizing different electrochemical reactions for unforeseen applications. One such example of major interest is the electrochemical water splitting process, for the production of pure hydrogen and oxygen gases. In spite of tremendous research efforts and major advancements in the field during the past decades, scarce efforts towards the visualization/imaging of the water splitting electrochemical reactions were invested. As a consequence, in this work, a universal approach for the in-situ spatiotemporal visualization of water splitting reaction under neutral water as well as neutral sea water conditions is performed (**Figure 1**). These two systems are specifically chosen to demonstrate universality of the technique developed by showcasing the potential applicability towards pH based visualization under neutral water (**Figure 2-4**) along with non

–pH change based, specific by-product visualization of chloride oxidation process (**Figure 7**) in neutral sea water electrolysis process. Furthermore, the influence of electrodes distance (**Figure 5**) and electrolyte flow rates (**Figure 6**) on the water splitting performance is analyzed visually, and directly related to the electrochemical performance of the electrolyser. The universality of the technique developed can further be explored for in-depth understanding of any electrochemical reactions including the highly anticipated intermediate chemical oxygen species influencing the well-known oxygen evolution/reduction reaction as an example<sup>51</sup>.

It is well established that under neutral water splitting, an enhancement in acidic and basic conditions takes place around anode and cathode, respectively, upon cell operation. This is usually considered detrimental for electrochemical water splitting<sup>52,53</sup>, however herein, we have explored this phenomenon as a benefit to perform direct spatiotemporal dynamic in-situ optical visualization of on-catalyst water splitting processes. For this purpose, we have explored the pH-sensitive fluorescent probe HPTS (**Figure 2**), directly as a homogeneous additional component in the electrolyte medium. and successfully visualized the electrochemical water splitting reactions. The fluorescent probe explored in this work is HPTS (8-hydroxypyrene-1,3,6-trisulfonicacid) that belongs to the pyrene-family. HPTS is a class of molecule called photoacid, which displays a change in its pKa ( $\sim 7.4$  to  $\sim 0.4$ ) thus, an acid - base transition between their ground and excited state<sup>48</sup>. The protonated and deprotonated forms of the HPTS molecule are shown in **Figure 2a, b** respectively. It is to be emphasised here that the protonated and the deprotonated forms of the HPTS molecule absorb at different wavelengths of  $\sim 400$  nm and  $\sim 450$  nm, respectively, thus allowing a ratiometric fluorescence analysis for accurately quantifying the pH changes occurring in a system, by analyzing the fluorescence at different excitation wavelengths. This forms the basis of choosing HPTS molecule as the fluorescent probe for the purpose of visualizing water splitting. The fluorescence spectrum (emission wavelength: 513 nm) of HPTS solution at neutral conditions (pH 7) shows two bands at  $\sim 400$  nm and  $\sim 450$  nm, corresponding to the protonated and deprotonated forms, respectively (**Figure 2c**).

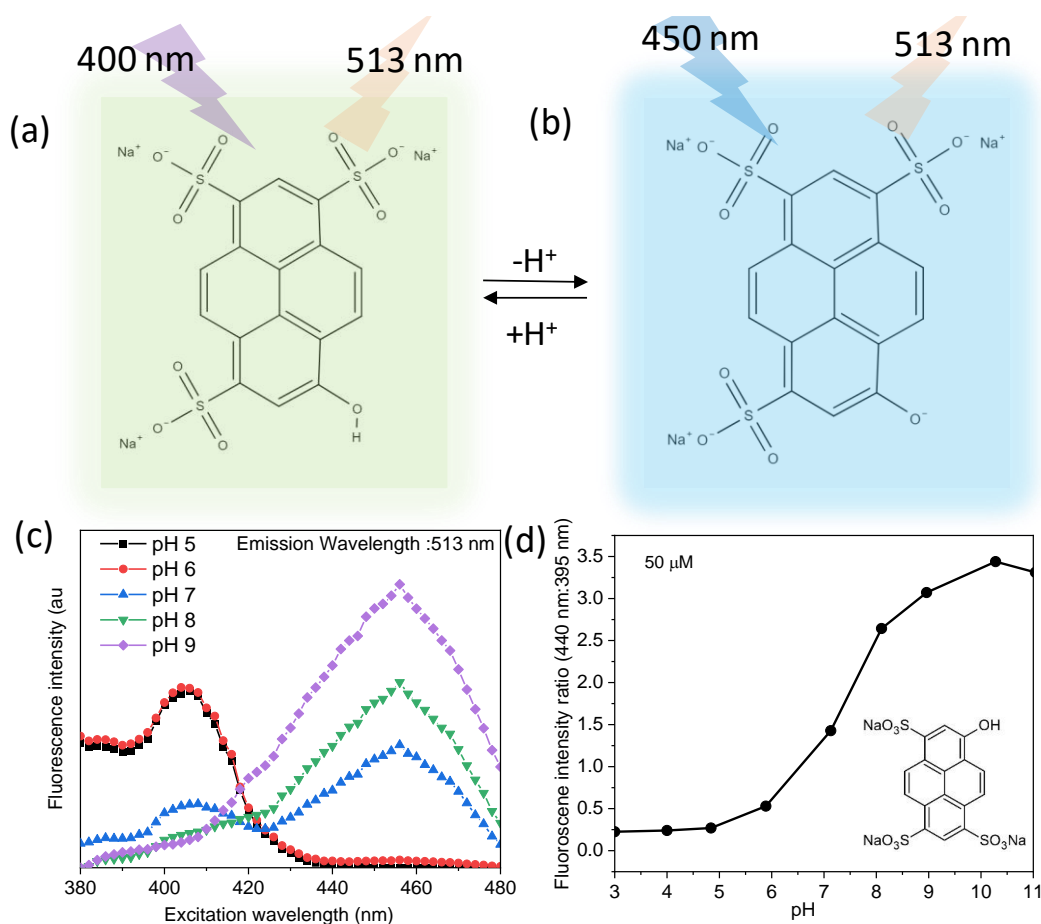


**Figure 2.** Chemical structure of the (a) protonated and (b) deprotonated forms of the fluorescent probe HPTS (8-hydroxypyrene-1,3,6-trisulfonic acid). (c) Fluorescence spectra (at 513 nm emission wavelength) of 50  $\mu\text{M}$  HPTS solution at different pHs (5-9) and (d) Fluorescence intensity ratio (excitation ratio 440 nm:395 nm) of HPTS solutions at different pHs.

Upon increasing or decreasing the pH, an increase or decrease in the band intensity is observed at  $\sim 450$  nm and  $\sim 400$  nm, respectively. Specifically, upon increasing the pH from 7, an increase in the band intensity at  $\sim 450$  nm is observed with a concomitant decrease in that at  $\sim 400$  nm. Similarly, upon decreasing the pH from 7, an increase in the band intensity at  $\sim 400$  nm is observed with a concomitant decrease in that at  $\sim 450$  nm. This optical property can be directly explored for pH sensing, and thus fluorescence imaging as a systematic ratiometric trend in the fluorescence ratio for excitation at 440 nm:395 nm is observed upon increasing the pH (**Figure 2d**). It is very important to notice that a sudden change in the fluorescence intensity ratio (ratiometric response) occurs upon any small deviation from neutralization (pH 7), and thus can be extremely sensitive for visualizing any minute pH changes inside the electrochemical cell upon operation.

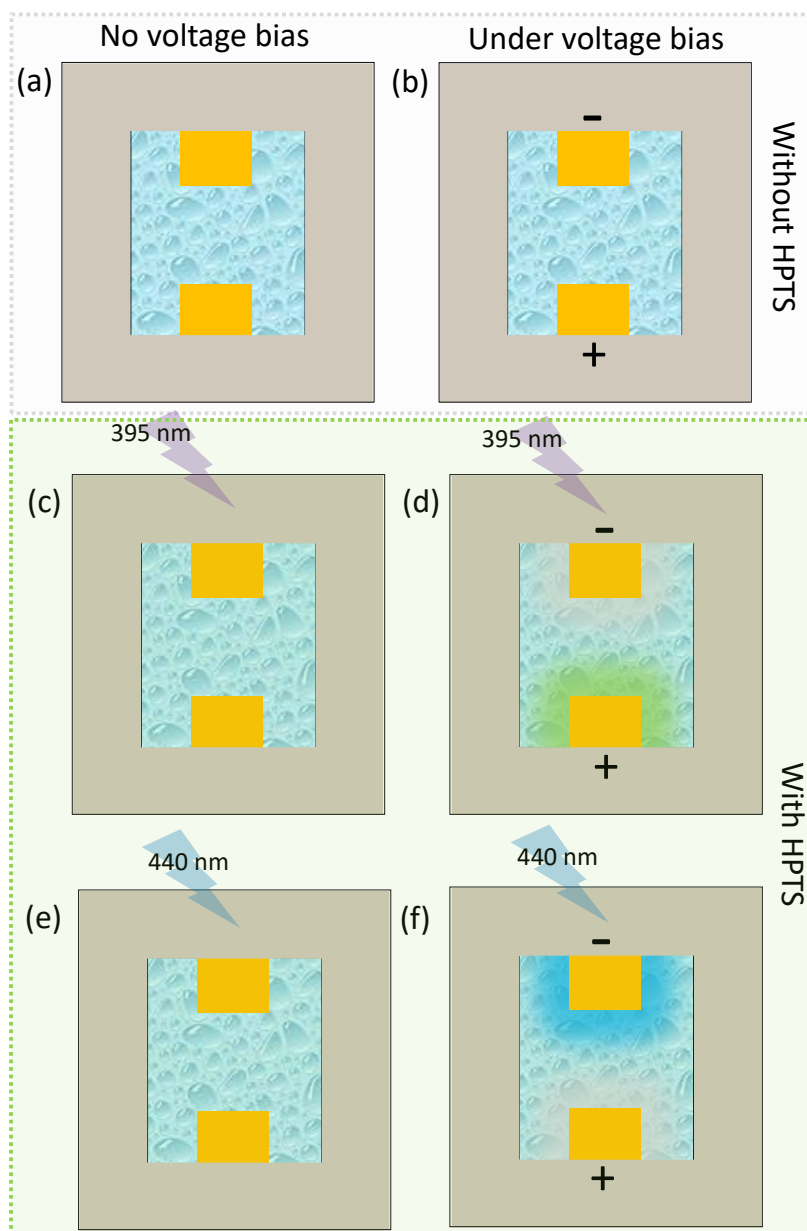


**Figure 3.** Schematic demonstration of the opto-electrochemical spatiotemporal cell imaging approach (a,b) without HPTS probe, (c,d) under 395 nm and (e,f) under 440 nm excitation wavelengths.

Due to the exceptional fluorescence properties of HPTS molecule, it was explored as a fluorescent probe that can be directly added to the electrolyte medium. However, at this point it is very important to analyse the electrochemical properties of the HPTS molecule to investigate its applicability in the electrochemical water splitting system. For this purpose, cyclic voltammetry was performed using a 0.25 M  $\text{Na}_2\text{SO}_4$  electrolyte, with and without the addition of 50  $\mu\text{M}$  HPTS probe, at a low scan rate of 5 mV/sec. Interestingly, it was observed that no oxidation or reduction peaks are observed, with an insignificant change in the cyclic voltammogram, in comparison to that for pristine electrolyte (Figure S1). This certainly qualifies the use of HPTS as a fluorescent probe in the opto-electrochemical water splitting cell

by direct addition in the electrolyte medium. As the HPTS molecule is demonstrated to be ‘electrochemically-inert’ in the voltage-window of interest, any change in the fluorescence properties of the electrochemical cell with HPTS as the fluorescent probe can be directly related to the changes occurring due to electrochemical production of hydrogen and oxygen. Hence, an electrochemical cell setup was assembled, with two electrodes at a specific distance, and with a transparent optical window that allows real-time fluorescence microscopy analysis. During electrochemical water splitting reaction under ‘unbuffered’ neutral conditions, upon application of a voltage greater than the onset potential, an increase/decrease in the pH is expected to occur at the cathode/anode compartments, respectively. However, without the addition of HPTS in the electrolyte, the change in pH cannot be visualized/analysed upon the application of voltage (**Figure 3 a,b**). In contrary, addition of HPTS as a fluorescent probe allows the detection of any change in the environment’s pH, and thus allows for the in-situ spatiotemporal visualization of the individual electrochemical water splitting reactions occurring at the cathode and anode, as well as their influence on the electrolyte bulk at any point inside the cell’s space. As HPTS displays two excitation wavelengths, specific for its protonated and deprotonated states (**Figure 2c**), the opto-electrochemical cell is exposed to 395 nm and 440 nm excitation wavelengths for analysing any resulting deviations in the local environment’s pH upon cell operation. Using 395 nm as the excitation wavelength shall display an increase/decrease in the fluorescence intensity at the vicinity of the anode/cathode due to an increase/decrease in the concentration of the protonated form of HPTS upon cell operation (**Figure 3c,d**). Similarly, excitation with a wavelength of 440 nm shall demonstrate an increase/decrease in the fluorescence intensity at the vicinity of the cathode/anode due to an increase/decrease in the concentration of the unprotonated form of HPTS upon cell operation (**Figure 3e,f**). Thus, for overall visualization of the electrochemical water splitting process, we performed a ratiometric image analysis in order to obtain a reliable and accurate pH visualization, with quantification of any known/unknown modulation in the electrochemical reaction.

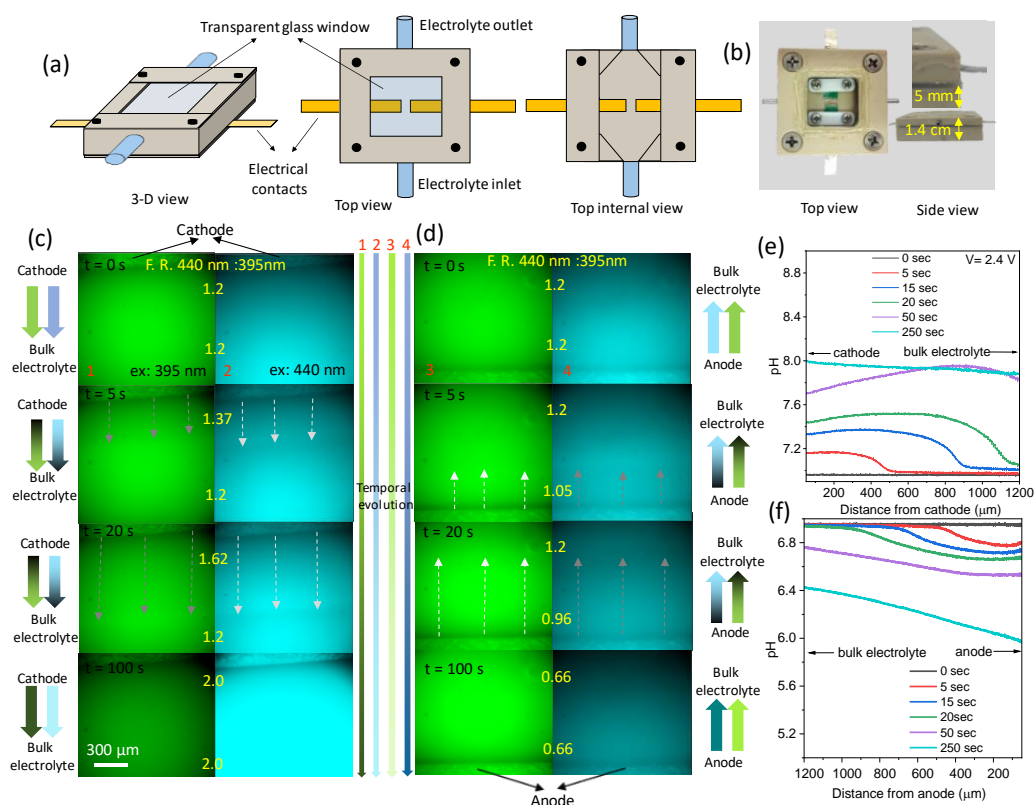


**Figure 4.** (a) Schematic demonstration and (b) digital photograph of the opto-electrochemical cell used in this work. Spatiotemporal fluorescence imaging of the (c) cathode and (d) anode vicinity under electrochemical cell operation at 2.4 V, using 50  $\mu\text{M}$  HPTS as fluorescent probe in 0.25 M  $\text{Na}_2\text{SO}_4$  electrolyte. pH variations around (e) cathode and (f) anode vicinity calculated via ratiometric analysis of c and d.

Based on the proposed hypothesis an opto-electrochemical cell was fabricated to perform the in-situ spatiotemporal dynamic optical visualization of on-catalyst water splitting processes. **Figure 4a** shows the schematics of the opto-electrochemical cell prototype developed and used in this study. The electrochemical cell consists of electrical contacts for the electrodes along with an optically transparent window. Also, electrolyte inlet and outlet ports are included for flowing the electrolyte inside the cell at controlled flow rates. A V-shaped inlet is provided in the cell geometry to minimize electrolyte flow turbulences and allow for smooth electrolyte flow. The distance of the electrodes surfaces from the optical window was minimized, keeping in mind the focal distance of the optical objective lens in use. Thus, an opto-electrochemical cell with an electrode-to optical window distance of 5 mm was fabricated as shown in the digital photograph shown in **Figure 4b**. The opto-electrochemical cell was filled with 0.25 M  $\text{Na}_2\text{SO}_4$  electrolyte along with 50  $\mu\text{M}$  of the HPTS fluorescent probe. The fluorescence imaging of the opto-electrochemical cell was performed using confocal microscopy under 395 nm and 440 nm excitation wavelengths. The fluorescence measurements were performed at a fixed voltage of 2.4 V, and the space volumes around the cathode (**Figure 4c**) and anode (**Figure 4d**)

are visualized in real-time. Before the application of any voltage, the electrolyte around the electrodes (both cathode and anode) does not show any pH changes, and thus no optical changes are observed, and exhibit a 440 nm:395 nm emission ratio of 1.2 (**Figure 4c**) at the electrodes surface as well as far from the electrodes surface (towards bulk electrolyte). As soon as the mentioned voltage is applied, due to the formation of acidic ( $H^+$ ) and basic ( $OH^-$ ) by-products around the cathode and the anode, respectively, a rapid change in the fluorescence intensity is observed. At the close vicinity of the cathode, a decrease/increase in the fluorescence intensity for excitation at 395 nm/440 nm is observed, due to the formation of alkaline conditions, leading to an increase in deprotonated form of the HPTS probe. As a result, an increase in the 440 nm:395 nm fluorescence ratio near the cathode is observed, with no changes observed away from the cathode's surface at 5 seconds after voltage operation. As the time for voltage operation is increased, an increase in the 440 nm:395 nm fluorescence ratio is observed (1.62 at 20 seconds), along with an increase in the space volume, or front width, where the effect of alkalinity is observed due to diffusion of  $OH^-$  species towards the bulk electrolyte from the cathode's surface. Similarly, the influence of acidification at the anode is observed, with the formation of a moving acidic front with increased voltage operation times, due to the diffusion of  $H^+$  species from the electrode towards the bulk (**Figure 4d**). As a result, with increasing voltage application time, a decrease in the 440 nm:395 nm fluorescence ratio is observed from 1.2 at 0 s, 1.05 at 5 s, 0.96 at 20 s and 0.66 at 100 s. The fluorescence ratios were further analyzed and calibrated to finally obtain the change in the pH around the electrodes surface, and the in-situ spatiotemporal evolution of electrolytic medium under water splitting conditions (**Figure 4e,f**). As expected, as soon as the potential is applied, an increase in the pH is observed around the cathode surface which further extends up to a distance of 400  $\mu m$  at 5 s (**Figure 4e**). The pH further increases and saturates at  $\sim$ pH 8 within 100 s, and extends to more than 1 mm distance from the electrode's surface, which was beyond the field of view of the objective lens. Similarly, a decrease in the pH was observed around the vicinity of the anode, which increases temporally, reaching a value of  $\sim$  pH 6 at 100 seconds (**Figure 4f**). As expected, the pH changes are at their maximum level at close vicinity of the electrodes surface, while the bulk electrolyte exhibit lesser deviation from neutrality, which is expected due to diffusion limitations. Thus, for the first time, direct in-situ spatiotemporal imaging of the chemical phenomena happening during water splitting processes is performed, and is in correlation with the previous literature knowledge. As a result, a reliable imagining technique for direct visualization of electrochemical water splitting reactions is successfully developed here.

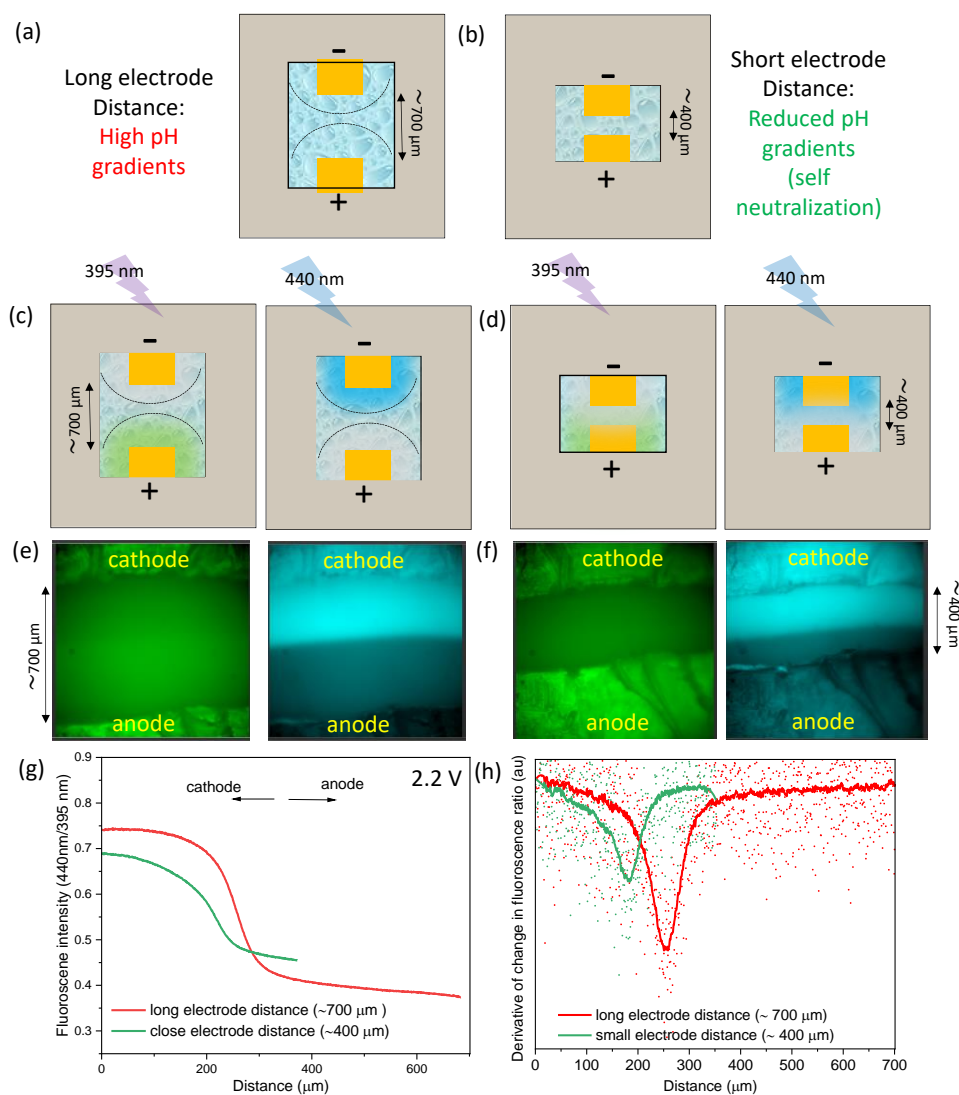


**Figure 5.** Schematics of the opto-electrochemical cell at (a) long and (b) short inter-electrodes distances without HPTS probe. Schematics demonstrating the fluorescence imaging of the opto-electrochemical cell at (c) long and (d) short inter-electrode distances with HPTS probe at excitation wavelengths of 395 nm and 440 nm. Fluorescence imaging of the opto-electrochemical cell at (e) long (~700  $\mu\text{m}$ ) and (f) short (~400  $\mu\text{m}$ ) inter-electrode distances with HPTS probe at excitation wavelengths of 395 nm and 440 nm. Ratiometric analysis demonstrating (g) change in the fluorescence ratio for short and long inter-electrode distances with (h) corresponding derivative plots for comparative analysis.

The fluorescence-based imaging technique developed in this study was applied for better understanding the water splitting electrochemical processes. The detrimental effect of the rapid and dramatic pH changes at the electrode surface is due to the poor OER and HER under acidic and basic conditions, respectively. At large inter-electrodes distances, the large increase or decrease in the pH at the electrodes surroundings will have a significant detrimental effect on the overall water splitting performance. However, the point of interest is if the electrodes are close enough, at certain inter-electrodes distances, that the acidic and basic fronts developing

at the anode and cathode can actually ‘self-neutralize’ each other, leading to enhanced an electrochemical behaviour as described in **Figure 5a,b**. We here demonstrated, visually in **Figure 4**, that the water splitting under neutral non-buffered conditions causes a rapid and sharp increase in the acidity/alkalinity at anode/cathode surfaces, however, the influence of distance between the electrodes is yet to be studied. For this purpose, two opto-electrochemical cells configurations were investigated, with different inter-electrode distances of  $\sim 700\ \mu\text{m}$  (far) and  $\sim 400\ \mu\text{m}$  (close), and the in-situ spatiotemporal visualization for the comparative resulting pH changes was performed under excitation wavelengths of 395nm and 440nm (**Figure 5 c,d**). Fluorescence spatiotemporal imaging shows that in both cases, far and close inter-electrodes distances, an increase/decrease in the fluorescence intensity around the electrodes is observed due to the formation of acidic/basic fronts at excitation wavelength of 395 nm and 440 nm. Interestingly, a clear difference in the electrolyte media characteristics around the cathode and the anode is observed with the bright and dark fluorescent phases merging at the centre point between the electrodes. These dark/bright phases are due to the formation of protonated and deprotonated forms of HPTS at the anode and cathode, respectively (**Figure 5e,f**). To understand the effect of decrease in the distance between the electrodes, the fluorescence images were ratiometrically analysed in-depth in order to see the comparative pH changes occurring at the electrodes at far and close inter-electrodes distances (**Figure 5 g**). The fluorescence intensity ratio (excitation at 440nm:395nm) for both far and close inter-electrodes distances demonstrates a highly stable response at close vicinity to the cathode surface, then decreases sharply towards the centre point between the electrodes and finally stabilizing close to the anode. This is expected due to the formation of acidic and basic environment spaces around the anode and cathode, respectively, during the electrochemical water splitting process. Interestingly, a lesser deviation in the fluorescence intensity is observed from cathode to anode at close electrode inter-distances. This was further confirmed by plotting a derivate plot of the fluorescence intensity, shown in **Figure 5g**, which clearly shows that a much higher deviation in the fluorescence intensity is observed when the cathode and anode are far, in comparison to when they are close to each other. These results clearly indicate towards a lesser deviation from neutrality when the electrodes are close to each other, due to a self-neutralization phenomenon, in comparison to the case when the electrodes are far from each other. Thus, the direct spatiotemporal visualization of water splitting at different inter-electrode distances provides a new practical direction to the enhanced non-buffered neutral water splitting, where the detrimental acidic or basic environment formation at the electrodes vicinity can be effectively

decreased or totally eliminated by keeping the electrodes at a certain close distance in order to attain self-neutralization, thus enhanced water splitting performances.

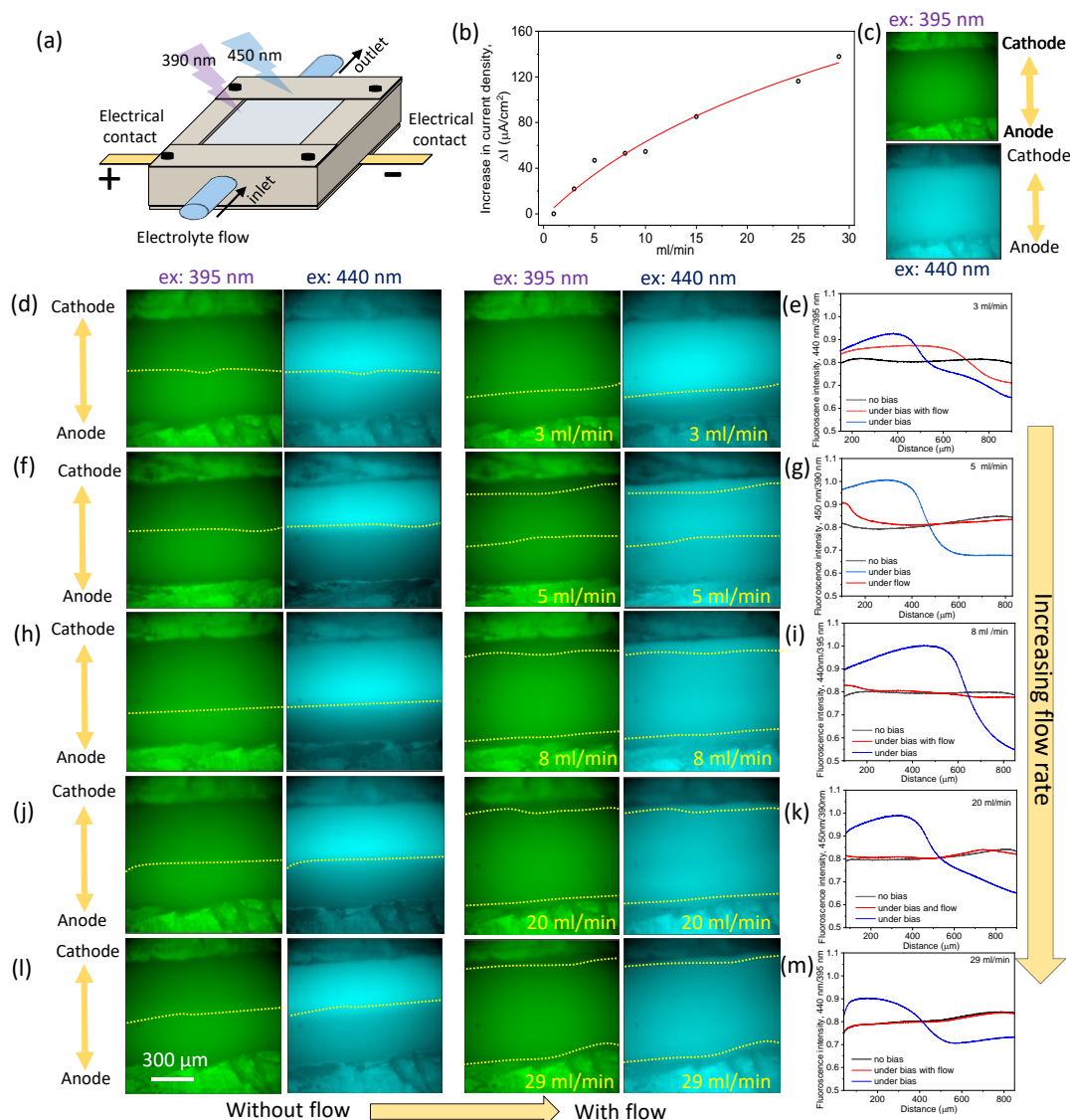


**Figure 6.** (a) Schematics of the opto-electrochemical flow cell for visualizing electrochemical water splitting processes under controlled flow conditions. (b) Increase in current density upon increasing the electrolyte flow rate. (c) Fluorescence imaging of the opto-electrochemical cell under buffered electrolytic conditions (0.25 M PBS). Fluorescence imaging at 395 nm and 440 nm excitation wavelengths, and corresponding ratiometric analysis of the opto-electrochemical cell under static and electrolyte flow rates of (d,e) 3 ml/min, (f, g) 5 ml/min, (h,i) 8 ml/min, (j,k) 20 ml/min and (l,m) 29 ml/min.

The detrimental effect of pH changes at the electrodes during water splitting under neutral conditions can also be minimized by replacing the water “shell” around the electrodes continuously. One plausible practical approach to do so is by flowing electrolyte in a flow-type electrolysis cell, which can provide in-situ 'buffering' conditions. The in-situ spatiotemporal

imaging technique developed in this study was explored to visualize the water splitting reactions under flow conditions. For this purpose, the opto-electrochemical cell developed in this work was equipped with flowing electrolyte capabilities, through the use of an external automated syringe pump (**Figure 6a**). To analyse the effect of different flow conditions on the electrochemical water splitting process, the change in the measured electrolyser's current under different electrolyte flow rates was investigated under static and flow conditions (**Figure 6b**). As expected, an increase in the electrolyser's current density was observed under flow conditions, in comparison to that observed under static electrolyte conditions. Interestingly, an increase in the electrolyser's current density was also observed with increasing electrolyte flow rates. The observed increase in the current density, ( $\Delta I$ ) rises rapidly at low flow rates, and then tend to stabilize at a certain plateau at increasing flow rates. To understand the increase in the electrolyser's current density at increasing flow rates, the in-situ visualization of the electrochemical water splitting cell under operation was performed under no-flow and under different flow rate conditions. As a control, the in-situ visualization of an electrolyser cell with 'buffering' electrolyte was performed under no-flow static conditions. As expected, no change in the spatiotemporal fluorescence imaging results was observed upon voltage application in the 'buffered' cell, as the corresponding acid and base by-products formed at the anode and cathode, respectively, are immediately and completely compensated by the externally used buffering agents in this control cell (**Figure 6c**). However, in non-buffered neutral medium, a clear spatiotemporal distinction in the fluorescence intensity, at cathode and the anode electrodes, for both 395 nm and 440 nm are observed due to the formation of basic and acidic space regions. To analyse the effect of flow on these acidic and basic conditions, the in-situ fluorescence imaging was performed under static and flow conditions at different flow rates (**Figure 6 d,f,h,j,l**). Furthermore, the spatiotemporal ratiometric analysis was performed to visualize any changes occurring upon voltage application, and the concomitant 'neutralization' effect happening upon flowing the electrolyte (**Figure 6 e,g,i,k,m**). Interestingly, under a very slow electrolytic flow condition of 3 ml/min (total cell exchange volume factor of 6 exchange/min), a considerable 'shrinking' in the acidic and basic space regions is observed, however, it can be observed that the acidic and basic space fronts are still clearly visible under these flow conditions (**Figure 6d**). The ratiometric analysis further demonstrates a clear spatiotemporal pH change upon the application of voltage (static condition, blue colour) in comparison to the non-bias condition (black colour). Upon flowing the electrolyte under a voltage bias, a lesser deviation in the fluorescence intensity ratio (440nm:395nm) is observed (red colour) in comparison to that for without flow (**Figure 6e**). Upon increasing the electrolyte

flow rate, a systematic decrease in the acidic and basic space fronts is observed, with the non-bias conditions slowly matching the results observed for flow conditions upon voltage bias application. Specifically, at a high flow rate of 29 mL/min (total cell exchange volume factor of 58 exchange/min), no acidic or basic space fronts are visible in the spatiotemporal fluorescence imaging, with the non-bias condition almost perfectly matching with that of bias application at high flow condition in the fluorescence intensity ratio plot (**Figure 6i,m**). Thus, the plot for increase in current density with the increase in flow rates can be directly related to the reduction, or complete inhibition, of the detrimental acidic and basic space fronts forming at the anode and cathode, respectively, upon electrolytic flow during the water splitting process. At low flow rate conditions, though the electrolyte is replaced at the electrodes surface, however, the electrolyte replacement rate is not sufficient to totally eliminate the dramatic spatiotemporal pH changes happening at the electrodes surface, leading to a significant increase in the electrolyser's current density. As the electrolyte flow rate is increased, a systematic decrease in the electrolyser's current density is observed, due to increased electrolyte replacement rate. At higher flow rates, the curve of the electrolyser's increase in current density reaches a plateau, because of at these high flow rates an effectively fast electrolyte replacement rate is attained, thus effectively inhibiting the formation of the detrimental acidic and basic space fronts at the electrodes vicinity during the water splitting process.

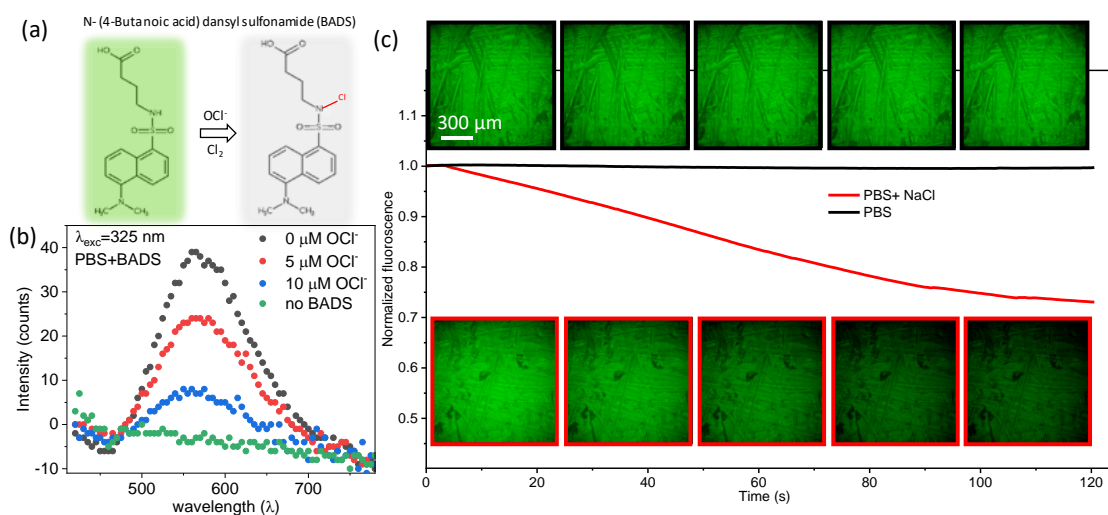


**Figure 7.** (a) Chemical structure of N-(4-butanoic acid) dansylsulfonamide (BADS) as a fluorescent probe for  $\text{OCl}^-/\text{Cl}_2$  detection and corresponding quenching of fluorescence upon interaction with  $\text{OCl}^-/\text{Cl}_2$  moiety. (b) Fluorescence quenching of 5  $\mu\text{M}$  BADS (at 325 nm excitation wavelength) solution in 0.25 molar phosphate buffer (pH7) using different

concentration of  $\text{OCl}^-$ . **(c)** Real time spatiotemporal imaging of chloride oxidation during artificial sea water electrolysis (at pH 7) at the electrode surface.

Inspired by the unprecedented application of imaging in-situ electrochemical reaction technique developed in this work, and to analyse the universality of the technique developed, we extended the work to visualize significantly different system by using a different fluorescent probe for detecting a specific product in the reaction rather than detection the pH change. As an example, the visualization of chloride oxidation at the anode during direct sea water splitting is temporally visualized using a dansylsulphoamide based fluorescent probe, N-(4-butanoic acid) dansylsulfonamide (BADs)<sup>54</sup> directly in the electrolyte during electrolysis. BADs is an exceptionally sensitive and selective fluorescent molecule which quenches upon interaction with  $\text{OCl}^-/\text{Cl}_2$  moieties even at very low concentrations as shown in **Figure 7a**. The optical properties and sensitivity towards  $\text{OCl}^-/\text{Cl}_2$  moieties was analysed by testing the excitation spectra of BADs with different concentration of hypochlorite ion ( $\text{OCl}^-$ ). It is important to realize that as observed in the previous sections water splitting under neutral conditions is prone to pH changes around the electrode and BADs is sensitive to pH changes, all the analysis was further performed in buffered neutral conditions to avoid any changes occurring due to the change in pH. The emission spectra of 5  $\mu\text{M}$  BADs at an excitation wavelength,  $\lambda_{\text{exc}} = 325$  nm shows a clear emission band centred at  $\sim 560$  nm. Interestingly, even with the addition of 5  $\mu\text{M}$   $\text{OCl}^-$ , a significant decrease in the fluorescence intensity is observed which decreases further on increasing the  $\text{OCl}^-$  concentration to 10  $\mu\text{M}$  as shown in **Figure 7b**. Thus, the ability of BADs to detect small concentrations of  $\text{OCl}^-$  under neutral conditions is demonstrated and can be further applied for imaging the in-situ oxidation of  $\text{Cl}^-$  during sea water splitting. For the purpose, BADs was directly used as a fluorescent probe in the opto-electrochemical imaging cell developed in this study for imaging chloride oxidation during sea water splitting. The BADs based opto-electrochemical cell with 0.5 M NaCl (artificial seawater) in buffered neutral electrolyte with Pt electrodes was operated at 3 V to ensure the oxidation of  $\text{Cl}^-$  to form  $\text{OCl}^-/\text{Cl}_2$  moieties at the anode. Hence, the spatiotemporal imaging of the anode was performed at  $\lambda_{\text{exc}} = 395$  nm at chronoamperometric conditions of 3V in electrolyte with and without 0.5 M NaCl (**Figure 7c**). The BADs in the electrolytic system demonstrates initial intrinsic fluorescence at the electrode surface. Remarkably, upon application of the external voltage, a decrease in the fluorescence intensity was observed due to the oxidation of  $\text{Cl}^-$  to  $\text{OCl}^-/\text{Cl}_2$ , which thereby quenches the intrinsic fluorescence of BADs. Interestingly, a systematic decrease in the overall fluorescence intensity was observed with increasing time because of the

systematic increase in the  $\text{OCl}^-/\text{Cl}_2$  concentration in the opto-electrochemical cell during electrolysis. Further, an insignificant change in the fluorescence intensity was observed upon electrolysis of PBS without NaCl, thus confirming the systematic decrease demonstrated in the in-situ visualization to the systematic oxidation of chloride ions which eventually quenches the fluorescence. As a result, opto-electrochemical imaging technique developed in this work was successfully extended to a significantly different (pH independent) electrochemical reaction using a totally different fluorophore. As an another example, Hydroethidine based fluorophore can be explored for visualizing and probing in-depth insights on the reactive oxygen intermediates which are known to influence the major energy based electrochemical reactions including the oxygen reduction and oxygen evolution reactions<sup>55-57</sup>.

Thus, the spatiotemporal imaging approach developed in this work has shown to be able to universally visualize in real-time, as never seen before, the on-electrodes electrochemical processes in the electrolyte itself. Importantly, the applicability of this proposed approach was successfully evaluated for practically realizing the 'self-neutralization' phenomenon via decreasing the inter-electrodes distance, and also for understanding the enhancing effects of electrolyte's flow on the overall electrochemical water splitting reaction performance. Furthermore, the use of  $\text{OCl}^-/\text{Cl}_2$  specific probes was successfully explored for imaging in-situ electro oxidation of  $\text{Cl}^-$  in sea water oxidation, remarkably justifying the universality of the technique developed for temporally visualizing any electrochemical reaction for in-depth unprecedented.

## Conclusions

In conclusion, a novel experimental paradigm for the in-situ spatiotemporal 'visualization' of electrochemical reactions, with water splitting applied as model system, is developed in this study. For this purpose, the photoacid molecule HPTS (8-hydroxypyrene-1,3,6-trisulfonicacid) is explored as a fluorescent probe for monitoring any spatiotemporal pH deviations occurring in the electrochemical system. The applicability of the opto-electrochemical platform developed in this work, was successfully evaluated in the real-time spatiotemporal analysis of the electrocatalytic water splitting reactions occurring under neutral electrolytic conditions. As a result, for the first time, the direct spatiotemporal dynamic in-situ optical visualization of on-catalyst water splitting processes is performed by adding a single fluorescent pH-probe directly into the electrolytic medium. Interestingly, the clear developing temporal formation of acidic and basic space environments around the anode and cathode, respectively, is observed, both concomitantly exhibiting a temporal increase in dimensions as a consequence of the enhanced

accumulation and diffusion of these formed acid and base by-products. The opto-electrochemical cell developed in this work was further explored to investigate and analyze for the first time the water splitting processes at neutral conditions. The in-situ spatiotemporal visualization of the water splitting processes at small electrodes inter-distances was successfully explored to unprecedentedly realize the possibility of 'self-neutralization' of the detrimental acidic and basic space fronts, at these small distances. Furthermore, the enhancement in the electrocatalytic water splitting activity under controlled flowing electrolyte conditions was thoroughly examined by the direct spatiotemporal visualization approach. It was clearly observed that at increasing electrolyte flow rates, a considerable decrease in the dimensions of the acidic and basic space fronts, formed during the water splitting process, is observed, thus decreasing, and finally completely inhibiting, the detrimental effects of the sharp pH changes occurring on the electrodes' vicinity during the performance of water splitting under neutral conditions. Furthermore, to demonstrate the universal extension of the experimental tool developed in this work to more specific reaction by products, direct in-situ visualization of  $\text{OCl}^-/\text{Cl}_2$  produced during electrolysis of sea water was successfully performed using N-(4-butanoic acid) dansylsulfonamide as a selective fluorophore. Thus, a unique opto-electrochemical spatiotemporal real-time universal visualization approach was successfully developed and demonstrated in this work, which holds the potential to open new fields of research and provide new impactful insights to the field of electrochemistry and its related applications.

### Acknowledgement

Authors acknowledge the mechanical workshop at Tel Aviv University for fabricating the opto-electrochemical cell prototype used in our studies.

### References

1. Filanovsky, B., Granot, E., Presman, I., Kuras, I. & Patolsky, F. Long-term room-temperature hydrazine/air fuel cells based on low-cost nanotextured Cu-Ni catalysts. *J. Power Sources* **246**, 423–429 (2014).
2. Harpak, N., Davidi, G. & Patolsky, F. Breathing parylene-based nanothin artificial SEI for highly-stable long life three-dimensional silicon lithium-ion batteries. *Chem. Eng. J.* **429**, 132077 (2022).
3. Harpak, N., Davidi, G., Cohen, A., Raz, A. & Patolsky, F. Thermally-treated nanowire-structured stainless-steel as an attractive cathode material for lithium-ion batteries. *Nano Energy* **76**, 105054 (2020).
4. Cohen, A. *et al.* Three-Dimensional Monolithically Self-Grown Metal Oxide Highly Dense Nanonetworks as Free-Standing High-Capacity Anodes for Lithium-Ion

- Batteries. *ACS Appl. Mater. Interfaces* **14**, 28911–28923 (2022).
5. Harpak, N. *et al.* Large-Scale Self-Catalyzed Spongelike Silicon Nano-Network-Based 3D Anodes for High-Capacity Lithium-Ion Batteries. *Nano Lett.* **19**, 1944–1954 (2019).
  6. Patolsky, F., Lichtenstein, A. & Willner, I. Electrochemical transduction of liposome-amplified DNA sensing. *Angew. Chemie - Int. Ed.* **39**, 940–943 (2000).
  7. Patolsky, F., Weizmann, Y. & Willner, I. Redox-active nucleic-acid replica for the amplified bioelectrocatalytic detection of viral DNA. *J. Am. Chem. Soc.* **124**, 770–772 (2002).
  8. Wu, Z. *et al.* Recent Progress of Vacancy Engineering for Electrochemical Energy Conversion Related Applications. *Adv. Funct. Mater.* **31**, 1–36 (2021).
  9. Teymourian, H. *et al.* Wearable Electrochemical Sensors for the Monitoring and Screening of Drugs. *ACS Sensors* **5**, 2679–2700 (2020).
  10. Mackanic, D. G., Chang, T. H., Huang, Z., Cui, Y. & Bao, Z. Stretchable electrochemical energy storage devices. *Chem. Soc. Rev.* **49**, 4466–4495 (2020).
  11. Baranwal, J., Barse, B., Gatto, G., Broncova, G. & Kumar, A. Electrochemical Sensors and Their Applications: A Review. *Chemosensors* **10**, (2022).
  12. Krivitsky, V., Filanovsky, B., Naddaka, V. & Patolsky, F. Direct and Selective Electrochemical Vapor Trace Detection of Organic Peroxide Explosives via Surface Decoration. *Anal. Chem.* **91**, 5323–5330 (2019).
  13. Alkhadra, M. A. *et al.* Electrochemical Methods for Water Purification, Ion Separations, and Energy Conversion. *Chem. Rev.* **122**, 13547–13635 (2022).
  14. Sumitha, M. S. & Xavier, T. S. Recent advances in electrochemical biosensors – A brief review. *Hybrid Adv.* **2**, 100023 (2023).
  15. Patolsky, F. & Lieber, C. M. Nanowire nanosensors. *Mater. Today* **8**, 20–28 (2005).
  16. Zheng, G., Patolsky, F., Cui, Y., Wang, W. U. & Lieber, C. M. Multiplexed electrical detection of cancer markers with nanowire sensor arrays. *Nat. Biotechnol.* **23**, 1294–1301 (2005).
  17. Lefler, S. *et al.* Multicolor Spectral-Specific Silicon Nanodetectors based on Molecularly Embedded Nanowires. *Nano Lett.* **18**, 190–201 (2018).
  18. Qazi, U. Y. Future of Hydrogen as an Alternative Fuel for Next-Generation Industrial Applications; Challenges and Expected Opportunities. *Energies* **15**, (2022).
  19. Wu, Y., Jamali, S., Tilley, R. D. & Gooding, J. J. Spiers Memorial Lecture. Next generation nanoelectrochemistry: the fundamental advances needed for applications. *Faraday Discuss.* **233**, 10–32 (2021).
  20. Brinkert, K. & Mandin, P. Fundamentals and future applications of electrochemical energy conversion in space. *npj Microgravity* **8**, (2022).
  21. Tao, S. *et al.* In Operando Closed-cell Transmission Electron Microscopy for Rechargeable Battery Characterization: Scientific Breakthroughs and Practical Limitations. *Nano Energy* **96**, 107083 (2022).
  22. Borberg, E. *et al.* Light-Controlled Selective Collection-and-Release of Biomolecules

- by an On-Chip Nanostructured Device. *Nano Lett.* **19**, 5868–5878 (2019).
23. Borberg, E., Granot, E. & Patolsky, F. Ultrafast one-minute electronic detection of SARS-CoV-2 infection by 3CLpro enzymatic activity in untreated saliva samples. *Nat. Commun.* **13**, (2022).
  24. Heifler, O. *et al.* Clinic-on-a-Needle Array toward Future Minimally Invasive Wearable Artificial Pancreas Applications. *ACS Nano* **15**, 12019–12033 (2021).
  25. Harpak, N., Borberg, E., Raz, A. & Patolsky, F. The ‘bloodless’ Blood Test: Intradermal Prick Nanoelectronics for the Blood Extraction-Free Multiplex Detection of Protein Biomarkers. *ACS Nano* **16**, 13800–13813 (2022).
  26. Bowyer, W. J., Xie, J. & Engstrom, R. C. Fluorescence imaging of the heterogeneous reduction of oxygen. *Anal. Chem.* **68**, 2005–2009 (1996).
  27. Bizzotto, D. In situ spectroelectrochemical fluorescence microscopy for studying electrodes modified by molecular adsorbates. *Curr. Opin. Electrochem.* **7**, 161–171 (2018).
  28. Doneux, T., Bouffier, L., Goudeau, B. & Arbault, S. Coupling Electrochemistry with Fluorescence Confocal Microscopy to Investigate Electrochemical Reactivity: A Case Study with the Resazurin-Resorufin Fluorogenic Couple. *Anal. Chem.* **88**, 6292–6300 (2016).
  29. Sojic, N. & Bouffier, L. Interplay between electrochemistry and optical imaging: The whole is greater than the sum of the parts. *Curr. Opin. Electrochem.* **34**, 101007 (2022).
  30. Rudd, N. C. *et al.* Fluorescence confocal laser scanning microscopy as a probe of pH gradients in electrode reactions and surface activity. *Anal. Chem.* **77**, 6205–6217 (2005).
  31. Yang, M., Batchelor-Mcauley, C., Kätelhön, E. & Compton, R. G. Reaction Layer Imaging Using Fluorescence Electrochemical Microscopy. *Anal. Chem.* **89**, 6870–6877 (2017).
  32. Fuladpanjeh-Hojaghan, B. *et al.* In-Operando Mapping of pH Distribution in Electrochemical Processes. *Angew. Chemie - Int. Ed.* **58**, 16815–16819 (2019).
  33. Peretz-Soroka, H. *et al.* Manipulating and Monitoring On-Surface Biological Reactions by Light-Triggered Local pH Alterations. *Nano Lett.* **15**, 4758–4768 (2015).
  34. Krivitsky, V. *et al.* Cellular Metabolomics by a Universal Redox-Reactive Nanosensors Array: From the Cell Level to Tumor-on-a-Chip Analysis. *Nano Lett.* **19**, 2478–2488 (2019).
  35. Li, X., Hao, X., Abudula, A. & Guan, G. Nanostructured catalysts for electrochemical water splitting: Current state and prospects. *J. Mater. Chem. A* **4**, 11973–12000 (2016).
  36. Yang, H., Driess, M. & Menezes, P. W. Self-Supported Electrocatalysts for Practical Water Electrolysis. *Adv. Energy Mater.* **11**, (2021).
  37. Chen, F. Y., Wu, Z. Y., Adler, Z. & Wang, H. Stability challenges of electrocatalytic oxygen evolution reaction: From mechanistic understanding to reactor design. *Joule* **5**, 1704–1731 (2021).
  38. Wu, Z. P., Lu, X. F., Zang, S. Q. & Lou, X. W. Non-Noble-Metal-Based Electrocatalysts toward the Oxygen Evolution Reaction. *Adv. Funct. Mater.* **30**, (2020).

39. Bahuguna, G., Cohen, A., Harpak, N., Filanovsky, B. & Patolsky, F. Single-Step Solid-State Scalable Transformation of Ni-Based Substrates to High-Oxidation State Nickel Sulfide Nanoplate Arrays as Exceptional Bifunctional Electrocatalyst for Overall Water Splitting. *Small Methods* **6**, 2200181 (2022).
40. Bahuguna, G., Verma, M. & Gupta, R. Chemical insights into electrophilic fluorination of SnO<sub>2</sub> for photoelectrochemical applications. *J. Mater. Chem. A* **9**, 19965–19974 (2021).
41. Bahuguna, G., Filanovsky, B. & Patolsky, F. Pioneering practical direct sea water splitting via an intrinsically-selective chlorine-phobic nickel polysulphide nanostructured electrocatalyst for pure oxygen evolution. *Nano Energy* **111**, 108439 (2023).
42. Bahuguna, G., Cohen, A., Filanovsky, B. & Patolsky, F. Electronic Structure Engineering of Highly-Scalable Earth-Abundant Multi-Synergized Electrocatalyst for Exceptional Overall Water Splitting in Neutral Medium. *Adv. Sci.* 2203678 (2022) doi:10.1002/advs.202203678.
43. Xu, Y., Wang, C., Huang, Y. & Fu, J. Recent advances in electrocatalysts for neutral and large-current-density water electrolysis. *Nano Energy* **80**, 105545 (2021).
44. Anantharaj, S. & Aravindan, V. Developments and Perspectives in 3d Transition-Metal-Based Electrocatalysts for Neutral and Near-Neutral Water Electrolysis. *Adv. Energy Mater.* **10**, 1–30 (2020).
45. Kim, B., Kim, T., Lee, K. & Li, J. Recent Advances in Transition Metal Phosphide Electrocatalysts for Water Splitting under Neutral pH Conditions. *ChemElectroChem* **7**, 3578–3589 (2020).
46. Yu, J. *et al.* A mini-review of noble-metal-free electrocatalysts for overall water splitting in non-alkaline electrolytes. *Mater. Reports Energy* **1**, 100024 (2021).
47. Shih, A. J. *et al.* Water electrolysis. *Nat. Rev. Methods Prim.* **2**, (2022).
48. Nandi, R. & Amdursky, N. The Dual Use of the Pyranine (HPTS) Fluorescent Probe: A Ground-State pH Indicator and an Excited-State Proton Transfer Probe. *Acc. Chem. Res.* **55**, 2728–2739 (2022).
49. Bahuguna, G. & Patolsky, F. Why Today's "Water" in Water Splitting is not Natural Water? Critical up-to-date Perspective and Future Challenges for Direct SeaWater Splitting. *Nano Energy* **117**, 108884 (2023).
50. Bahuguna, G. & Patolsky, F. Enabling Unprecedented Ultra-Efficient Practical Direct Seawater Splitting by Finely-Tuned Catalyst Environment via Thermo-Hydrodynamic Modulation. *Adv. Energy Mater.* **2301907**, 1–12 (2023).
51. Hao, Y. *et al.* Chemical oxygen species on electrocatalytic materials during oxygen evolution reaction. *Mater. Today Catal.* **2**, 100012 (2023).
52. Shinagawa, T., Ng, M. T. K. & Takanabe, K. Electrolyte Engineering towards Efficient Water Splitting at Mild pH. *ChemSusChem* **10**, 4155–4162 (2017).
53. Obata, K., Van De Krol, R., Schwarze, M., Schomäcker, R. & Abdi, F. F. In situ observation of pH change during water splitting in neutral pH conditions: Impact of natural convection driven by buoyancy effects. *Energy Environ. Sci.* **13**, 5104–5116

- (2020).
54. Wei, Y. Determination of chlorine by fluorescence quenching. (2000).
  55. Wang, Y., Jia, S., Yu, Z., Wen, H. & Cui, H. Insights Into the Detection Selectivity of Redox and Non-redox Based Probes for the Superoxide Anion Using Coumarin and Chromone as the Fluorophores. *Front. Chem.* **9**, 1–11 (2021).
  56. Papapostolou, I., Patsoukis, N. & Georgiou, C. D. The fluorescence detection of superoxide radical using hydroethidine could be complicated by the presence of heme proteins. *Anal. Biochem.* **332**, 290–298 (2004).
  57. Gomes, A., Fernandes, E. & Lima, J. L. F. C. Fluorescence probes used for detection of reactive oxygen species. *J. Biochem. Biophys. Methods* **65**, 45–80 (2005).